Cycle network model of Prostaglandin H Synthase-1

Alexey Goltsov [1,2,], Maciej Swat[3], Kirill Peskov[1,4], Yuri Kosinsky[1]*

[1] *M&S Decisions LLD, Moscow, Russia*

[2] *Russian Technological University (MIREA), Moscow, Russia*

[3]*Simcyp PBPK Modeling and Simulation, Certara, Sheffield, United Kingdom*

[4]*Computational Oncology Group, I.M. Sechenov First Moscow State Medical University, Moscow, Russia*

[*]Corresponding author: Alexey Goltsov, e-mail: alexey.goltsov@msdecisions.ru

Abstract

The kinetic model of Prostaglandin H Synthase-1 (PGHS-1) was developed to investigate its complex network kinetics and non-steroidal anti-inflammatory drugs (NSAIDs) efficacy in different *in vitro* and *in vivo* conditions. To correctly describe the complex mechanism of PGHS-1 catalysis, we developed a microscopic approach to modelling an intricate network dynamic of 35 intraenzyme reactions among 24 intermediate states of the enzyme. The developed model quantitatively describes interconnection between cyclooxygenase and peroxidase enzyme sites; substrate (arachidonic acid, AA) and reducing cosubstrate competitive consumption; enzyme self-inactivation; autocatalytic role of AA; enzyme activation threshold, and synthesis of intermediate PGG_2 and final PGH_2 products under wide experimental conditions. In the paper we provided the detailed description of the enzyme catalytic cycle, model calibration based on a series of *in vitro* kinetic data and model validation using experimental data on the regulatory properties of PGHS-1.

The validated model of PGHS-1 with an unified set of kinetic parameters is applicable for *in silico* screening and prediction of the inhibition effects of NSAIDs and their combination on the balance of pro-thrombotic (thromboxane) and anti-thrombotic (prostacyclin) prostaglandin biosynthesis in platelets and endothelial cells expressing PGHS-1.

Keywords: PGHS-1, COX-1, NSAID, network model, enzyme regulation.

1. Introduction

Prostaglandin H synthase-1 (PGHS-1) also known as Cyclooxygenase-1 (COX-1) catalyses the first stage in the conversion of arachidonic acid (AA) into prostaglandin H_2 (PGH_2) being precursor of physiologically active prostanoids [19]. PGHS-1 together with the other isoform of PGHS, PGHS-2 are the main targets of non-steroidal anti-inflammatory drugs (NSAIDs) in treatment of pain, fever, inflammation, and cardiovascular diseases [15]. Despite the fact that this enzyme has been under thorough investigation for several decades, some details of its catalytic mechanism still remain not completely understood [22]. It is generally recognized that PGHS-1 has two distinct catalytic activities: a cyclooxygenase (COX) activity converting AA to an intermediate product, prostaglandin G_2 (PGG_2) and a peroxidase (POX) activity which further converts PGG_2 into a final product PGH_2. PGHS-1 catalysis represents a complex network of many oxidized/reduced reactions connecting multiple enzyme intermediates and leading to redox transformation of key catalytic components such as AA binding site (COX site) and heme-prosthetic group (POX site). Another not completely understood phenomena in PGHS-1 catalysis is so-called self-inactivation process, including gradual decay of both COX and POX activities during PGHS-1 catalysis [25]. Commonly, two different catalytic mechanisms have been suggested to account for the range of experimental data observed in PGHS-1 catalysis: Branched-Chain (BC) mechanism [5] and alternative Tightly Coupled (TC) mechanism [1]. In the framework of these two mechanisms, several various mathematical models have been proposed to elucidate the details of PGHS-1 catalysis.

According to the BC mechanism of the PGHS-1 catalysis, supported by much experimental data, PGHS-1 catalyses oxygenation of AA to prostaglandin PGH_2 in two sequential stages in distinct enzyme sites (Fig. 1). At the first stage, Tyr385 radical, the oxidants in the COX active site, abrogates a hydrogen atom from AA to activate the reaction of AA oxygenation to the transient product, endoperoxy hydroperoxide prostaglandin G (PGG_2). At the second step of the catalysis, PGG_2 is reduced to the final product, endoperoxyalcohol PGH_2 in the heme prosthetic group of the POX-site of the enzyme. The TC mechanism of PGHS-1 catalysis [1] suggests that the POX and COX activities are tightly coupled, and peroxidase compound in the POX-site activities AA oxygenation without requirement of Tyr radical formation in the COX-site.

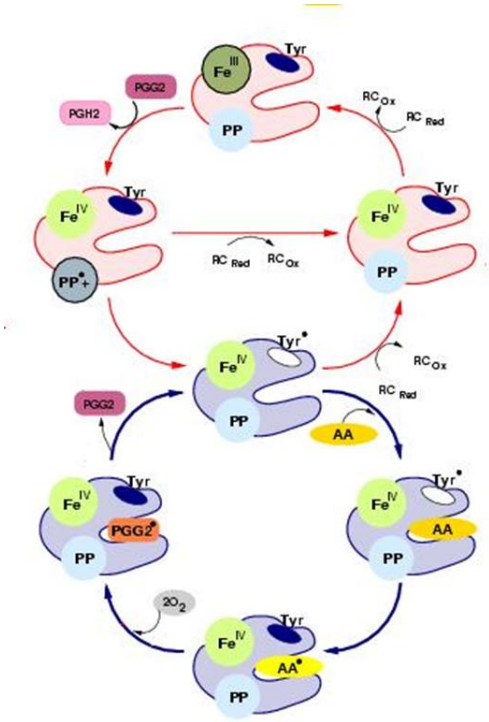

Fig. 1. Scheme of the Branched Chain mechanism of PGHS -1 catalysis [5]. *Detailed description of all the enzyme states is given in Table 1.*

The most detailed mathematical models of PGHS-1 have been developed in a series of papers [24], [14], [2]. These kinetics models were based on the assumptions of BC mechanism of PGHS-1 function, and gradually evolved starting from eight reactions in an initial model [24] to 22 reactions in the latest version [2]. An increase in the complexity of the models reflected a growing insight into the mechanism of catalysis and molecular structure of PGHS-1, and mainly resulted from introduction of additional enzyme intermediates and reactions into these proposed catalytic schemes and more detailed consideration of enzyme self-inactivation. Each step in a gradual refinement of the model and an increase in its complexity were supported by the new experimental data as it became available. The developed models allowed satisfactorily describing the key features of PGHS-1 catalysis, i.e. interaction of POX and COX activities, self-inactivation and autocatalytic effect, as well as estimating key kinetic constants of the PGHS-1 reaction mechanism [4].

Abundance of accumulated experimental data on the PGHS-1 kinetics stimulated development of many various kinetic models of PGHS-1. Several other models of PGHS-1 have been developed with a view to describe individual datasets and explain certain peculiarities of PGHS-1 functioning. For example, the kinetic models of PGHS-1 developed by Vrzheshch et al. [23] allowed qualitatively describing sets of experimental data on AA, O_2

and RC consumption under specific *in vitro* conditions. The kinetic models of two isoforms, PGHS-1 and PGHS-2 were developed to explain the differences in their kinetics and activation thresholds [9].

None of the existing mathematical model of PGHS-1 can provide quantitative description of all key regulatory effects within a unified set of kinetic parameters. In the other words, different models and sets of parameters should be used to reproduce accurately a wide spectrum of experimental data on PGHS-1 and predict its function *in vivo* in health and pathological conditions. It complicated significantly the use of the existing models of PGHS-1 for *in silico* study of inhibition effect of NSAIDs in different *in vitro* and *in vivo* conditions, and for their application in the development of Quantitative Systems Pharmacology (QSP) models, where prostaglandins pathway is one of the drug targets.

In spite of great progress in a qualitative and quantitative modelling of PGHS-1 the problem of quantitative description of the main experimental facts on the reaction mechanism of PGHS-1 as well as the reproduction of experimental data obtained in different *in vitro* and *in vivo* conditions in the framework of a unified kinetic model is still remaining. The new experimental data appears and adds new knowledge on the enzyme structures which can play a role in prostaglandin biosynthetic unknown up to the present [29].

Basing on the ideas of BC mechanism [5], and their realisation in the kinetic models [2, 14, 24], in this paper we developed the microscopic kinetic approach to modelling a complex network dynamics of intraenzyme reactions among multiple catalytically active intermediate states of the enzyme to represent the detailed kinetic mechanisms of PGHS-1 function. This model has been previously applied to the description of *in silico* NSAID action alone and in combination and showed satisfactory predictive results [6, 7]. But many aspects of the model and features of the interaction of NSAIDs and PGHS-1 have remained beyond the scope of these publications. In this paper we give a full description of the model assumptions, method of its parametrisation, validation, and model application to the analysis of experimental data on regulatory properties of PGHS-1. One of the main aims of this work is the construction of reliable and validated kinetic model of PGHS-1, which would incorporate current theoretical conceptions on PGHS-1 function and would be capable to reproduce quantitatively much experimental data on prostaglandin biosynthesis in the framework of a unified set of kinetic parameters.

2. Results

2.1. Development of the catalytic cycle of PGHS-1

The derivation of the model of PGHS-1 catalysis represents a special task, as both POX and COX activities are known to be located in different enzyme domains within the same protein complex and that these activities can proceed independently of each other [11]. Another important feature of PGHS-1 catalysis is that it involves intramolecular electron transfer and formation of multiple redox and binding states of the catalytic domain. The start point of our modelling was the BC mechanism [5], [14] schematically represented in Fig.1. The full catalytic cycle of PGHS-1 includes two distinct catalytic activities: a cyclooxygenase (COX) activity converting arachidonic acid (AA) to an intermediate product, prostaglandin G2 (PGG_2), and a peroxidase (POX) activity, which further converts PGG_2 into final product PGH_2. Following the approach to the PGHS-1 modelling [14], we assumed that PGHS-1 catalysis could be presented as a network of microscopic reactions, each of them resulting in a corresponding change in the enzyme catalytic state. Under catalytic state we understand the state of PGHS-1 catalytic domain, which in its turn is defined by a unique combination of the states of its key elementary catalytic constituents, located in the COX and POX active sites. In our model we considered the following key catalytically active components: fatty acid binding site (COX site), heme prosthetic group (POX site) and Tyr385 residue in the COX site. The COX site we defined through the presence/absence of AA in the hydrophobic channel of COX region. The POX state was determined by the redox states of heme iron and protoporphyrin group. Tyr385 residue was assumed to exist in either ground or radical state. In addition, we considered states of fully inactive enzyme, FIE [26]. The detailed description of all-possible states for each catalytic component, considered in our model, is given in Table 1.

Fig. 2 shows kinetic scheme for the developed catalytic cycle of PGHS-1. The scheme is mainly based on the assumptions of the BC mechanism [5] and its further extension [14]. Additionally, we also included in the model some reactions corresponding to the TC mechanism [1]. Thus, our scheme represents a generalisation of two previously discussed catalytic mechanisms, and the results obtained in the framework of the model allowed us to draw the conclusions on the role of each mechanism in PGHS-1 catalysis.

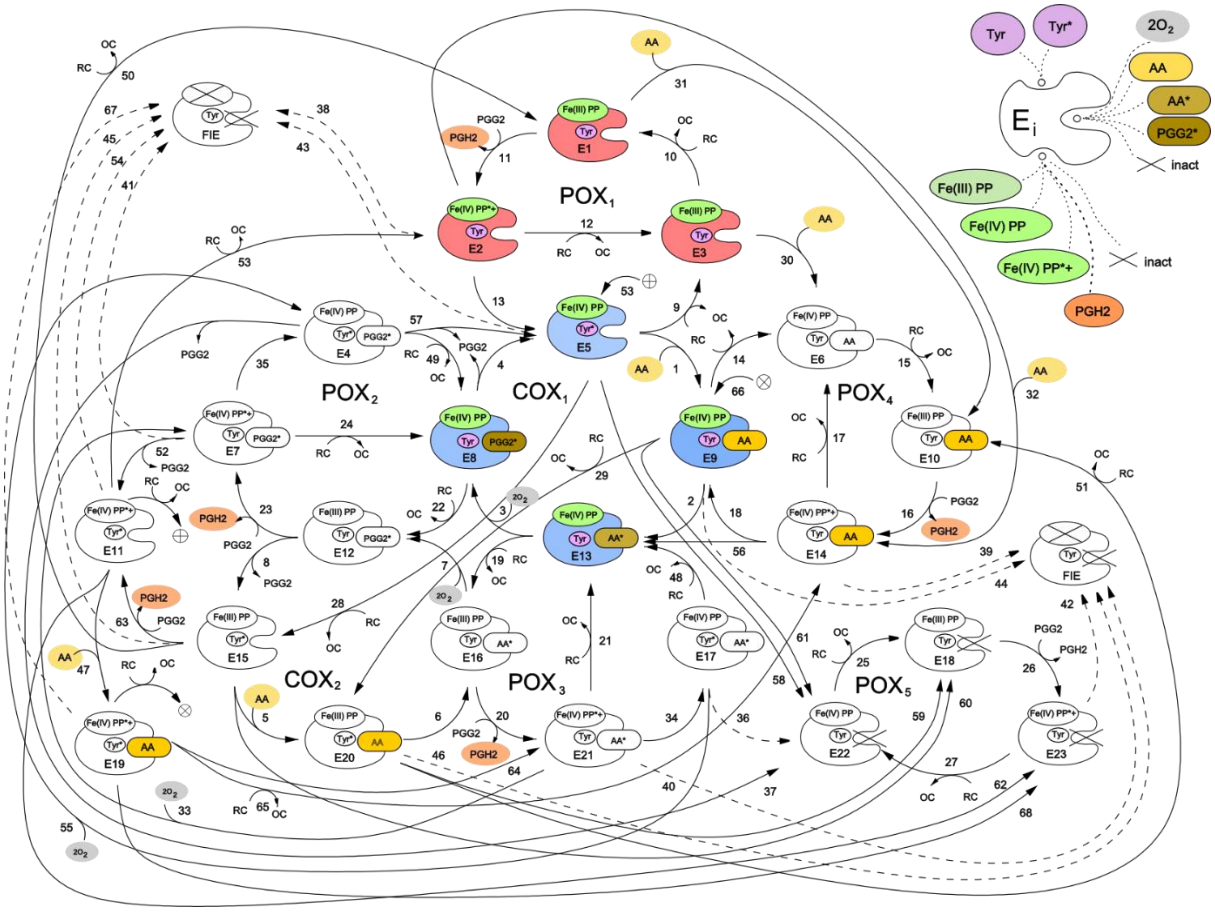

Fig. 2. Cycle network model of PGHS-1. Detailed description of all the enzyme states is given in Table 1. Enzyme states marked by colour correspond to the Branched Chain mechanism [5].

Table 1. Microstates of PGHS-1 considered in the model.

n	Catalytic components	N	Notation of the states	Description of the states
1	Heme prosthetic group (POX site)	1	Fe(III), PP	Protoporphyrin group in ground state;
		2	Fe(IV), PP*+	Oxiferryl state of Fe (Fe(IV)=O) and radical cation state of protoporphyrin group;
		3	Fe(IV), PP	Oxiferryl state of Fe (Fe(IV)=O) and reduced protoporphyrin group
2	Tyrosine 385	1	Tyr	Tyrosine residue
		2	Tyr*	Tyrosyl radical
3	AA binding site (COX-site)	1	empty	No ligands in the COX-site
		2	AA	Arachidonic acid in the COX site
		3	AA*	Arachidonyl radical in the COX site
		4	PGG_2*	Prostaglandin G_2 radical in the COX site
		5	FIE	Fully Inactive Enzyme

For convenience of consideration, we have presented the full catalytic cycle of PGHS-1 as a composition of eight interlinked cycles, five of them (POX_i) corresponding to the POX

activity, the other three (COX_j) – to the COX activity of the enzyme. In general, the full catalytic cycle of PGHS-1 can be considered as a complex dynamic network of elementary reactions which describes the totality of possible transitions between multiple states of the PGHS-1 catalytic domain.

Two interconnected cycles, COX_1 (reactions 1-4) and POX_1 (reactions 9-13) correspond to the BC mechanism. According to this mechanism, PGHS-1 catalysis is initiated in the POX site, and it's first step is the reaction of the resting enzyme state [Fe(III), PP] (E_1) with PGG_2 producing PGH_2 and leaving the heme prosthetic group in the state [Fe(IV), PP*+] (E_2). The enzyme state containing heme with two oxidizing equivalents – one on the iron and another one on the porphyrin radical cation – is referred to as Intermediate 1 [5]. In our model, we described this stage of POX catalysis by bimolecular irreversible reaction (reaction 11) of the resting state with PGG_2, resulting in production of PGH_2 and leaving the enzyme in the E_2 with heme in [Fe(IV), PP*+] state. E_2 state can be converted back to the resting state E_1 by 2 consecutive reactions with RC by followed release of oxidized cosubstrate, OC (reactions 12 and 10). Alternatively, E_2 state can undergo one-electron internal reduction via intramolecular electron transfer from Tyr385 to protoporphyrin (reaction 13) resulting in the formation of the E_5 state [Fe(IV), PP, Tyr^*] containing Tyr385 radical and a ferryl heme. This state is referred to as Intermediate II [5]. E_5 state can also complete POX cycle and return to the resting state E_1 via reactions 9 and 10 with RC through the formation of [Fe(IV), PP] referred as Compound II [5]. According to the BC mechanism, the presence of Tyr385 radical is ultimately required for AA oxidation in the COX site. Therefore, the intermediate state E_5 can potentially serve as a starting point for the further cascade of COX reactions.

The majority of previously known models included COX activity as a single Michaelis-Menten type reaction without considering its mechanism in any detail [2], [9]. In contrast, in our model we describe COX activity by four consecutive reactions (reactions 1-4 in COX_1 cycle) corresponding to the transitions of the enzyme through three intermediate enzyme-substrate complexes (E_9, E_{13} and E_8). Note that using of Michaelis-Menten approximation to describe the individual reactions involved in a reaction network is not strongly valid.

Reaction 1 describes reversible binding of AA with the enzyme state, E_5 resulting in the formation of the state [Fe(IV), PP, Tyr^*, AA] (E_9), containing AA in the COX site. Reaction 2 corresponds to the abstraction of a hydrogen atom from AA by Tyr385 radical and formation of the E_{13} state containing AA radical in the COX site, [Fe(IV), PP, Tyr, AA*]. Further AA^* reacts with two oxygen molecules and the intermediate product PGG_2^* radical is produced (reaction 3). We assumed that binding of the first and second oxygen molecules is a rapid

process, during which the redox state of the heme remains unchanged [24]. The final step of the COX_1 cycle in our model is irreversible reaction 4, which describes the process of regeneration of Intermediate II with Tyr385* radical (E_5), accompanied by the release of the intermediate product PGG_2 from the COX site.

Taking into account that POX activity of PGHS-1 is observed to proceed independently from COX catalysis [11], we considered possibility of several additional POX and COX catalytic cycles, originating from intermediate states of the POX_1 and COX_1 cycles. For example, in the COX_1 cycle, heme prosthetic group remains in the state [Fe(IV), PP] with one oxidising equivalent on iron, and therefore each of the enzyme states E_5, E_8, E_9, and E_{13} can potentially participate in redox reactions with RC (reactions 19, 22, 28, and 29), producing catalytic states E_{12}, E_{15}, E_{16}, and E_{20}. The later states can be considered as intermediates of an additional COX_2 cycle. Note that similar COX cycle was included in the model developed by Kulmacz et al. [11]. The COX_2 cycle differs from the COX_1 cycle only by the state of heme prosthetic group in the enzyme intermediates. Similarly, each intermediate of POX_1 cycle has an empty COX binding site, which allows for binding of AA (reactions 30, 31 and 32) and production of the states E_6, E_{10} and E_{14}, respectively. These states can participate in the POX_2 cycle, which differs from the POX_1 cycle by presence of AA in the COX binding site of its enzyme intermediates. Note, that binding of AA to the resting state (E_1), containing Tyr385 in the ground state, was considered in the PGHS-1 model for the first time, as all previously known models assumed, that AA binds solely to the enzyme containing Tyr385 radical state (Intermediate II, E_5). This allowed us to analyse how the redox state of key catalytic components can influence the enzyme binding with AA.

The third COX_3 cycle though not explicitly shown in the scheme, can be defined as a cycle formed by the enzyme states E_{11}, E_{19}, E_{21}, and E_7, involving in reactions 47, 64, 33, and 53, respectively. The reactions in the COX_3 cycle are initiated in the result of AA binding to the enzyme being in two-radical state [Fe(IV), PP*+, Tyr*] (state E_{11}). Note, that similar COX cycle was considered in the extended BC mechanism model [2], [11], but its contribution to PGHS-1 functioning was not indicated.

Using similar approach, we introduced into our model the POX_3 and POX_4 cycles, intermediates of which differ from POX_1 intermediates by the occupancy of the COX binding site – it contains AA radical in the POX_3 cycle and PGG_2 radical in the POX_4 cycle. The POX_5 cycle was included to account for remaining POX activity when the COX site is inactivated (see more detailed description below).

In our model, we also included an alternative route for initiation of COX reactions, which corresponds to the TC mechanism [5] - a direct hydrogen atom abstraction from AA by protoporphyrin radical cation PP*+ and generation of AA radical. In our scheme this mechanism is described by the reaction of AA binding to the initial state E_1 resulting in the production of enzyme-substrate complex E_{14}, [Fe(III), PP, Tyr, AA], which further converts into intermediate, [Fe(IV), PP, Tyr, AA*] (E_{13}) containing arachidonyl radical, AA* (reaction 56).

It should be mentioned that as opposite to this in BC mechanism, generation of AA* radical (which is an initiator of COX reaction) requires firstly the generation of Tyr385* radical state ([Fe(IV), PP, Tyr*] or Intermediate II) from Intermidiate I ([Fe(IV), PP*+, Tyr]). Intermediate II further binds AA which results in the formation of the AA* radical state [Fe(IV), PP, Tyr, AA*] (E_{13}).

Thus, in BC and TC mechanisms, COX activity originates from the different enzyme states – from radical state [Fe(IV), PP, Tyr*, AA] (Intermediate II with AA bound in the COX site) in BC mechanism, whereas in TC mechanism – from the state [Fe(IV), PP*+, Tyr, AA] (Intermediate I with AA in COX site). Consideration of two alternative mechanisms of AA* radical formation in our model allowed us to analyse their possible contributions to overall COX activity.

2.2. Modelling of PGHS-1 self-inactivation

Both POX and COX activities of PGHS-1 undergo irreversible self-inactivation (SI) during catalysis [26]. The exact mechanism of this process remains not completely understood [22]; however, there is a consensus that SI most likely originates from the enzyme damage caused by oxidative reactions, coming from certain radical intermediates generated in PGHS-1 [27]. Potentially, any enzyme intermediate containing oxidising equivalents or radicals can cause the enzyme damage. One of the key questions discussed in the literature is which intermediate states can serve as the origin for POX and COX inactivation.

Based on the experimental data we considered several possible mechanisms for enzyme SI in our model. These mechanisms included separately inactivation of the COX and POX activities, originating from enzyme intermediates with different redox state of heme group, and states containing one or two radicals in the catalytic domains [27]. All the SI processes accounted for in our model can be conditionally classified into the following groups:

1. Inactivation of POX activity resulting in fully inactivation enzyme (FIE state in Fig. 2). SI of POX activity in the BC mechanism leads to the subsequent loss of COX activity, as peroxydase reactions are required to regenerate Tyr385 radical state. In our model, this SI mechanism is described by reactions 43-46 and 54. Due to simplicity reasons, we did not distinguished two stages in this process and approximated it by one-stage irreversible first order reactions:

a) Reactions 38-42, 53, and 67 originate from Intermediate I and lead to POX and further COX inactivation due to radical state of heme prosthetic group ([Fe(IV),PP*+]) [20], [12]. In our model this process of enzyme inactivation can initiate from seven catalytic states containing radicals: E_2, E_7, E_{11}, E_{14}, E_{19}, E_{21}, and E_{23};

b) Reactions 43-46 originate from Intermediate II: states E_5, E_9, E_{15}, and E_{20} and lead to POX and further COX inactivation due to the presence of oxidising equivalent Fe(IV) in heme.

2. Direct inactivation of COX activity with remaining POX activity which can be caused by the presence of radical states in the COX catalytic site [26]. In our model the remaining POX activity is described by the POX_5 cycle (reactions 25-27). Similar POX cycle was considered in the model developed by Kulmacz et al. [11]. According to this hypothesis, we assumed that COX inactivation can originate from enzyme intermediates containing either one or two radicals in the COX catalytic site. Reactions 58-62, and 68 originate from the states containing one Tyr* radical in the COX site (E_5, E_9, E_{11}, E_{15}, E_{19}, and E_{20}), reactions 36 and 37 - from the states with two radicals in the COX site, [Fe(IV),PP, Tyr*, AA*] (E_{17}) and [Fe(IV),PP, Tyr*, PGG2*] (E_4). It should be noted that remaining POX activity can also further be inactivated due to damage caused by presence of radical state in heme (reaction 42).

2.3. Identification of a set of kinetic parameters of PGHS-1

As the result of joint fitting of three series of the experimental data (see Methods), the unified set of kinetic parameters was determined. The results of fitting are shown in Fig. 3 and presented in Table 2. For the comparison of the obtained kinetic constants of PGHS-1 with the results of other authors, we also included in the Table 2 experimental and theoretical estimations of the corresponding rate constants available from literature.

First, note that experimental values of the kinetic parameters were available just for a few elementary reactions within the PGHS-1 catalytic cycle. Such a lack of reliable experimental values is caused by practical impossibility of direct measurement of some reaction rates, for example, intramolecular electron transfer within the PGHS-1 complex. As seen from Table 2,

the identified values were close to those obtained experimentally where such data were available, for example, rate constants k_5, k_6, k_7, and k_9.

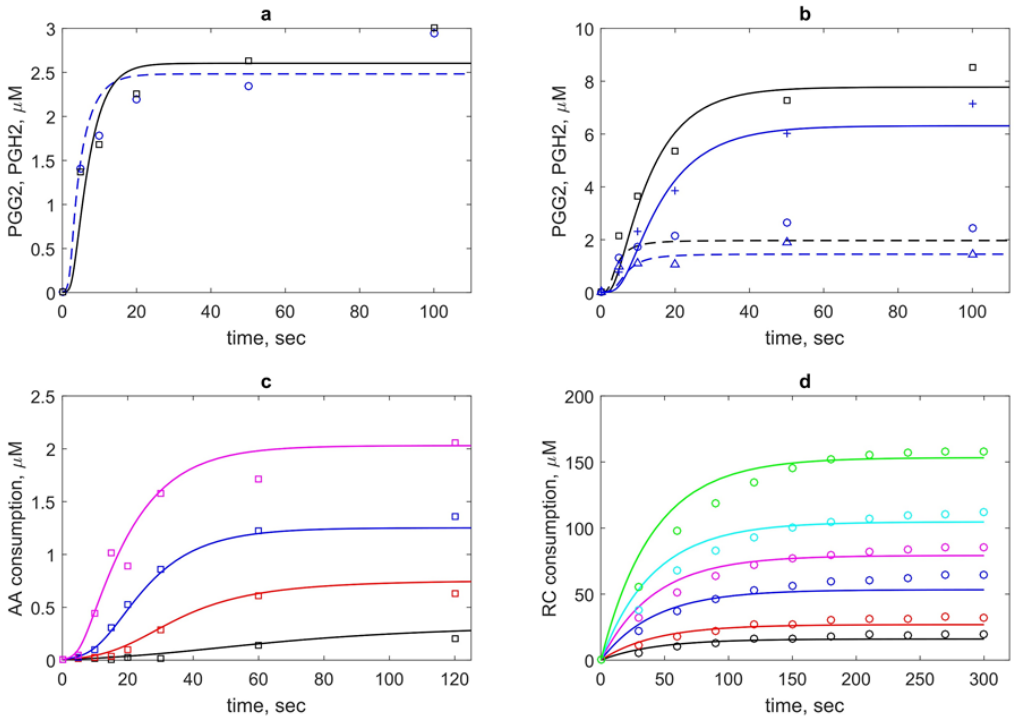

Fig. 3. PGHS-1 model calibration (lines) based on in vitro data on purified PGHS-1 kinetics (points). (a) Kinetics of PGG_2 (dash blue line) and PGH_2 (black solid line) at 100 μM phenol. (b) Kinetics of PGG_2 (dash lines) and PGH_2 (solid lines) at 1000 μM (blue lines) and 5000 μM (black lines). Theoretical and experimental data [24] *(a and b) obtained at 80 μM and 35 nM PGHS-1; (c) Theoretical and experimental* [4] *kinetics of AA consumption at 0.5 μM (black line), 1 μM (red line), 2 μM (blue line), and 20 μM (magenta line) PGHS-1 and 1 mM phenol. (d\|) Accumulation kinetics of oxidised RC (adrenochrome) at 0.32 μM (black line), 0.54 μM (red line), 1.08 μM (blue line), 1.62 μM (pink line), 2.16 μM (cyan line), and 3.22 μM (green line) adrenaline (RC) and 1.05 mM H_2O_2 Point – experimental data* [23].

As a result of fitting, the values of the dissociation constants of AA binding to the COX-site, $K_{d,1}$ (reaction 1 in the COX_1 cycle) and $K_{d,12}$ (reaction 12 in the COX_2 cycle) were estimated (Table 2). The only experimental estimate available for the stage of AA binding to PGHS-1 is the value of Michaelis constant (K_m = 3 μM -5 μM [19]. However, Michaelis constant is an apparent value and generally depends on the concentration of the second PGHS-1 substrate, RC (see discussion below), and therefore cannot be directly compared with $K_{d,1}$.

One of the key kinetic parameters of the PGHS-1 catalysis is the reaction rate of intramolecular electron transport from the heme group to the Tyr385 in the COX-site leading to the formation of Tyr385* radical. The obtained value for this constant k_9=310 s^{-1} is in close agreement with theoretical estimate 310 s^{-1} [11].

Table 2. Kinetic parameters of the PGHS-1 model.

Reactions	Kinetic constants	Values	Experimental or modeling data
COX reactions			
E_5+AA	k_1	690 μM^{-1} s^{-1}	
	$K_{d,1}$	0.1 μM	
AA → AA*	k_2	2690 s^{-1}	
AA*+$2O_2$	k_3	173 μM^{-2} s^{-1}	
PGG_2*+Tyr	k_4	13 s^{-1}	
POX reactions with RC (phenol) and PGG_2			
Tyr*+RC	k_5	0.18 μM^{-1} s^{-1}	0.001-0.1 μM^{-1} s^{-1} [25]
Fe(IV)+RC	k_6	0.58 μM^{-1} s^{-1}	0.53 μM^{-1} s^{-1} (4 ^oC) [10]
E+PGG_2	k_7	7.1 μM^{-1} s^{-1}	14 (1 ^oC); 35 (20 ^oC) [5]; 21 (25 ^oC) μM^{-1} s^{-1} [12]
Fe(IV*)+RC	k_8	0.001 μM^{-1} s^{-1}	
Fe(IV)+Tyr → Fe(IV)+Tyr**			
	k_9	310 s^{-1}	300 s^{-1} [12]
Reactions in POX_2 cycle			
Tyr*+RC	k_{10}	0.1 μM^{-1} s^{-1}	
Fe(IV*)+Tyr	k_{11}	1.1 s^{-1}	
AA binding to the resting enzyme, E_1			
E_1+AA	k_{12}	690 μM^{-1} s^{-1}	
	$K_{d,12}$	0.6 μM	
Fe(IV)+AA → IV+AA**			
	k_{13}	18.8 s^{-1}	
Self-inactivation reactions			
COX_{inact}	k_{15}	0.72 s^{-1}	0.1 s^{-1} [25]
POX_{inact}	k_{in1}	0.7 s^{-1}	0.2 – 0.5 s^{-1} (24 ^oC) [25]
COX_{inact}	k_{in2}	2.5 s^{-1}	0.22 s^{-1} [25]
POX reactions with adrenaline and H_2O_2			
	k_5	0.06 μM^{-1} s^{-1}	
	k_6	0.001 μM^{-1} s^{-1}	
	k_7	0.001 μM^{-1} s^{-1}	0.44 μM^{-1} s^{-1} (6.7 ^oC) [1], 0.01 μM^{-1} s^{-1} (1 ^oC), 0.028 (20 ^oC) [5]
	k_8	0.001 μM^{-1} s^{-1}	

Satisfactory quality of the fitting was achieved at the same values of kinetic parameters of COX activity for similar stages in all the three COX_i cycles considered in the model. Note that the COX_1, COX_2 and COX_3 cycles in the model differ only by the state of the heme prosthetic group in the POX site (see discussion in section 2.1). The independence of kinetic constants of the reactions in the COX site on the state of the heme group can indicate the absence of cooperativity between the POX and COX sites.

As the result of fitting, we estimated the rate constants for the different mechanisms of PGHS-1 self-inactivation (Table 2). As discussed in section 2.2, we considered three possible

mechanisms of SI in the model. For SI originating from Intermediate I ([Fe(IV),PP*+]), we obtained the value of the rate constant k_{in1}=0.6 s^{-1} which is in good agreement with experimental data [25] (Table 2). For SI originating from Intermediate II ([FeIV PP, Tyr*]), a higher value of the rate constant was determined k_{in2}=2.5 s^{-1}, which is consistent with the estimation of transition rate from Intermediate II to Intermediate III (state leading to full enzyme inactivation), 0.5 s^{-1}-2 s^{-1} [25]. For the reactions of COX inactivation (reactions 36, 37, 58-62, and 68) with the remaining POX activity (POX_5 cycle) we obtained rate constant k_{in}=0.72 s^{-1} (Table 2).

The small reaction rate k_8 of the reduction of protoporphyrin group radical state (Intermediate I, [Fe(IV), PP*+], E_2) by RC was obtained to be about zero k_8 (0.001 μM^{-1} s^{-1}) that means that the Intermediate I is rather reduced by intramolecular process of electron abstraction from Tyr385 with radical formation than by exogenous RC.

To estimate uncertainty of the parameters obtained in the fitting of the model against experimental data we carried out global sensitivity analysis (GSA) of the model (see Methods). The results of GSA revealed that the calibrated model showed uniformed sensitivity to the most kinetic parameters (Fig. 4). The model is weakly sensitivity to rate parameter k_{12} of the reactions of AA binding to the states in the POX_2 cycle (E_1, E_2 and E_3), while it is sensitive to the dissociation constant $K_{d,12}$ of the same reactions. The model also showed weak sensitivity to parameter k_{in2} which corresponds to one of the SI reactions of the enzyme, but it is highly sensitive to the parameters k_{in1} and k_{15} characterising the other SI reactions considered in the model.

The model satisfactory describes the experimental data on a pure POX activity of PGHS-1 which was induced by H_2O_2 in the presence of adrenalin as RC [23] (Fig. 3d). As the result of fitting, values of the kinetic parameters (k_5, k_6 and k_8) of the POX cycle of PGHS-1 treated by H_2O_2 and adrenalin (RC) were obtained to be less than those of POX reactions activated by PGG_2 in the presence of phenol (Table 2). This result is consistent with experimental data on the pure POX activity of PGHS-1 in the presence of different peroxides and cosubstrates [1, 5].

As seen from obtained agreement between theoretical and experimental data (Fig. 3), the model with the unified set of kinetic parameters satisfactorily described the various experimental data such as kinetics of intermediate PGG_2 and final PGH_2 products, as well as consumption of substrate, AA and cosubstrate, RC. The model with the obtained set of parameters given in Table 2 was further validated and applied to analysis of regulatory mechanisms of PGHS-1 catalysis.

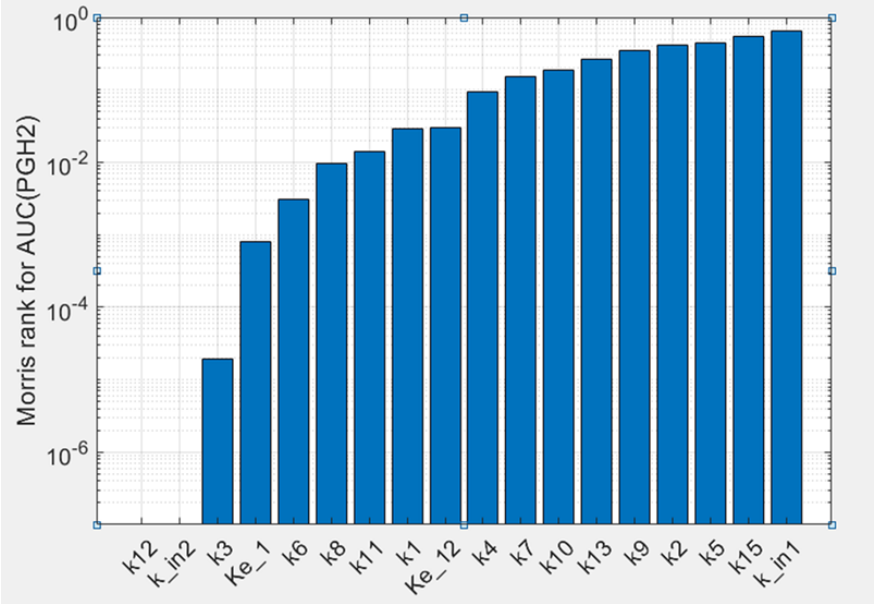

Fig. 4. Results of the global sensitivity analysis of the PGHS-1 model. Sensitivity of PGH_2 production to the kinetic parameters calculated as Morris rank [16] *for area under the curve (AUC) of the PGH_2 time series.*

2.4. Contributions of the different enzyme intermediates and intraenzyme reactions to PGHS-1 catalysis

The catalytic cycle of PGHS-1 (Fig. 2) represents a complex network of intermolecular states with intricate distribution of internal fluxes between them. To realise key intermediate states of the enzyme and fluxes, which contribute significantly to the PGHS-1 catalysis, we carried out a comparative analysis of the population distribution of intermediate enzyme states and fluxes. This allowed us to estimate relative impact of different elementary reactions and enzyme intermediates to the overall PGHS-1 function. We determined preferred ways of AA binding to the enzyme, identified key reactions producing intermediate PGG_2 and final product PGH_2, estimate the contribution of the different POX and COX cycles as well as compared the role of different mechanism of enzyme SI.

As mentioned above, in the model, we considered two possible ways of initiation of the COX reaction, namely two alternative ways of formation of the enzyme-substrate complex containing both Tyr385* radical and AA. The first way corresponds to a generally accepted mechanism of the COX reaction initiation in the BC mechanism, when formation of Intermediate II state [Fe(IV),PP, Tyr*] (E_5) precedes the binding of AA (reaction 1). The

second, alternative, mechanism is the binding of AA to the COX site (reactions 30-32) which can be followed by formation Tyr385* radical state, E_9 through reaction 18 (Fig. 2).

The performed flux analysis showed that AA binds to the Intermediate II (E_5) state much more effectively than to the resting state (E_1), Intermediate I (E_2) and E_3 state. Maximum flux $V_1(t)$ exceeds maximum values of $V_{30}(t)$, $V_{31}(t)$ and $V_{32}(t)$ by an order of magnitude (see comparison $V_1(t)$ and $V_{31}(t)$ in Fig. 3a. Note, that the reaction rate of AA binding to the resting enzyme (V_{31}) has a high peak in an initial stage of the COX reaction, but its contribution to overall catalysis is negligible because of short duration of the peak (1 ms).

The results of modelling also showed that the rate constant of electron transfer from Tyr385 residue to heme group depends significantly on the presence of AA in the COX site (reactions 13 and 18). The rate constant k_9 of reaction 13 going between enzyme states with the empty COX site equals to 300 s^{-1}, but the constant of reaction 18 between states with an occupied COX site k_{11} is lower than 10 s^{-1}. Thus, the reduction of heme group due to Tyr385* radical formation in the presence of AA in the COX site occurs weaker than that in the case of the empty COX site. Therefore, substrate-enzyme complex [Fe(IV), PP, Tyr*, AA] (E_9) is formed mainly from Compound II [5].

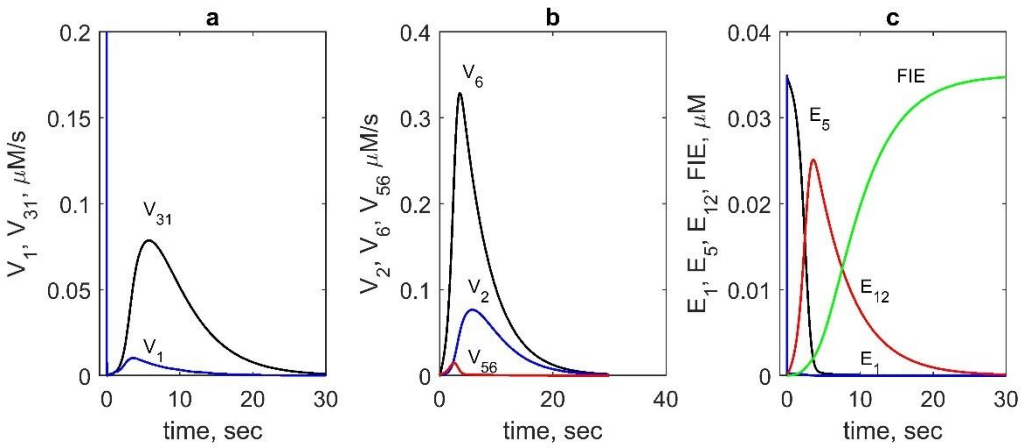

Fig. 5. Contributions of different reactions and enzyme intermediates to PGHS-1 catalysis obtained in the model. (a) Reaction rate of AA binding with E_5 state (V_1, blue line) and the resting state E_1 (V_{31}, black line). (b) Reaction rate of AA radical formation: V_2 (blue line), V_6 (black line) and V_{56} (red line). In calculation: 0.035 μM PGHS-1, 80 μM AA and 100 μM RC. (c) Kinetics of the main intermediates: E_1 (blue line), E_5 (black line), E_{12} (red line), FIE (green line).

To determine what COX_i cycles contribute significantly to the overall COX reaction, we compared the reaction rates of the PGG_2 synthesis in various COX_i cycles (Table 3) at the different concentration of RC (10 μM, 100 μM and 1000 μM). It turned out that the key COX

cycle in which maximum amount of PGG_2 is produced is COX_2 cycle (reaction 8). Recall that in our model heme group of the COX_2 cycle is in the ground ferric state [Fe(III),PP], as opposite to the kinetic models of PGHS-1 [5, 14], where heme group is assumed to remain in the unreduced ferril state [Fe(IV), PP] throughout COX reaction (COX_1 cycle in our model).

Calculation of the reaction rates showed that COX_1 cycle plays a significant role only at low concentrations of RC <10 μM (Table 3). This effect results from the increasing connection between COX_1 and COX_2 cycles that causes the reduction of heme group in the COX_1 cycle by RC (reactions 19, 22, 28, and 29) and a decrease of the role of the COX_1 cycle in overall catalysis. Additionally, the COX_2 cycle significantly contributes to the activation of AA oxygenation reaction in comparison with the COX_1 cycle. We also compared the rates of AA radical formation due to abstraction of a hydrogen atom from AA by Tyr385* radical in both COX cycles (Fig. 5b). The reaction rate V_6 in the COX_2 cycle was found to be significantly higher than the corresponding rate V_2 in the COX_1 cycle. We also compared contribution of two different reactions of AA radical formation which can happen either due to the Tyr385 radical according to the BC mechanism of PGHS-1 catalysis or due to another oxidant, oxyferryl heme, according to TC mechanism. The calculation showed that the reaction rate V_{56} of AA* formation owing to oxyferryl heme electron-transfer (TC mechanism) significantly lower that the corresponding reaction V_6 proceeding due to Tyr385 radical (BC mechanism) (Fig. 5b).

Calculation also showed that a significant contribution to catalysis of intermediate product, PGG_2, was made by the reaction of PGG_2* output from the E_4 state in the POX_2 cycle and its following reduction to PGG_2 in solution (reaction 57). Note, this reaction was included in the model according to the TC mechanism.

Table 3. Reaction rates of PGH_2 and PGG_2 production (μM/s) in the different POX_i and COX_i cycles at the different concentrations of RC.

RC, μM	V_{11}, POX_1	V_{16}, POX_2	V_{23}, POX_4	V_4, COX_1	V_8, COX_2	V_{52}, COX_3	V_{57}	Connection of COX_1 and COX_2 cycles		
								V_{22}	V_{28}	V_{29}
10	0.01	0.05	0.2	0.35	0.4	$7\cdot10^{-3}$	0.13	3.35	10^{-3}	10^{-3}
100	0.01	0.05	0.3	0.07	0.63	0.01	0.13	6.94	$5\cdot10^{-3}$	$5\cdot10^{-3}$
1000	0.01	0.06	0.5	0.01	0.69	0.02	0.03	10.55	0.01	0.01

To analyse the main reactions contributing considerably to PGH_2 synthesis, we calculated the fluxes in the POX_i cycles, in which PGH_2 is produced (Table 3). The main contribution to PGH_2 production turned out to be made by reaction 23 in the POX_4 cycle. Note that in the

PGHS-1 models developed based on the BC mechanism, PGH_2 is produced in reaction 11 in the POX_1 cycle. By contrast, in our model, reaction rate V_{11} is negligibly weak in comparison with reaction rate V_{23} (Table 3). To analyse this effect, we calculated the population kinetics of the enzyme states. Fig. 5c shows the time dependence of population of the states, maximum contributing to the PGHS-1 catalysis. These results showed that the POX_1 cycle contributes noticeably at the initial stage of PGH_2 synthesis when the population of the resting state of the enzyme is maximum. In contrast, state E_{12} in the POX_4 cycle works throughout all the catalysis, indicating that the POX_4 cycle is active up to full SI of PGHS-1. Moreover, state E_{12} ([Fe(III), PP, Tyr, PGG*] being common for the COX_2 and POX_4 cycles participates simultaneously in the production of intermediate product, PGG_2 (reaction 23) as well as the final product PGH_2 (reaction 8). As discussed above, these reactions make maximum contributions to the synthesis of PGG_2 and PGH_2 (Tables 3). Thus, in our model, COX_2 and POX_4 cycles are the main ones in PGHS-1 catalysis, while the COX_1 and POX_1 cycles contribute only at the initial stage of the PGHS-1 function.

2.5. Model application to the investigation of regulatory role of AA and RC in PGHS-1 function

The calibrated model was applied to study dependence of the PGHS-1 activity on substrate AA and cosubstrate RC concentrations. For comparison of the theoretical results with experiments we used validation experimental data which was not used in the fitting procedure. The comparison of model and experiment results obtained without any optional fitting was a validation test for the predictive power of the model to be applied it to the analysis of *in vivo* experimental data on the NSAD action.

First, we applied the model to calculate the dependence of the oxygen consumption rate on AA concentration, $V_{O2}(AA)$. For this, we first calculated kinetics of oxygen consumption rate, $V_{O2}(t)$ and compared the results with experimental data [24] (Fig. 6a). As seen, the model satisfactory describes experimental data on $V_{O2}(t)$ and reproduces the time of the enzyme activity, about 20 sec that is in agreement with the SI time of PGHS-1 [19]. To plot the dependence of $V_{O2}(AA)$, we took the maximum values of the rates $V_{O2}(t)$ calculated at different AA concentrations. The theoretical dependence of $V_{O2}(AA)$ along with experimental data [4] are given in Fig. 6b.

We also calculated $V_{O2}(AA)$ at different RC concentrations (Fig. 6b). As seen, RC inhibits COX activity of the enzyme, i.e. an increase in RC concentration leads to an increase of apparent Michaelis constant, K_m, and decrease of the maximum oxygen consumption rate. This means that AA and RC compete each other for the COX site according to reactions 1 and 9 in the catalytic cycle (Fig. 2). Based on these results we calculated the dependence of the Michaelis constant K_m for AA on RC concentrations (Fig. 6c). The range of theoretical values of K_m embraces a wide range of the experimental values of Michaelis constant, 3 μM-5 μM [19], [14] and 10.2 ± 1.5 μM [21]. Note that dissociation constants of AA binding with the enzyme obtained in our calculation is significantly lower, $K_{d1,AA}$ = 0.1 μM than K_m (Table 2).

The linear dependence K_m(RC) looks like the dependence of apparent Michaelis constant for a substrate on competitive inhibitor concentration, where RC plays a role of inhibitor: $K_m=K_d(1+RC/K_i)$. This relationship shows that when RC concentration approaches zero, the Michaelis constant K_m tends to the dissociation constant K_d of the substrate (AA). In our model dissociation constant $K_{d,1}$ =0.1 μM is close to the value of $K_m \approx 0.2$ μM at zero concentration of RC.

In the model, RC competes with AA for binding to the COX site, i.e. state E_5 in COX_1-cycle (reactions 1 and 9) and state E_{15} in the COX_2-cycle (reactions 5 and 50). According with BC mechanism, redaction of Tyr385* radical by RC leads to inhibition of COX activity.

Moreover, the discussed mechanism may explain the significant distinction of the obtained kinetic constants of the reduction rate of Tyr385* radical depending on a state of the COX site. In the parameter set (Table 2), the rate constant k_{10} of reactions 14 and 51 of Tyr385* reduction in the states E_9 (COX_1 cycle) and E_{20} (COX_2 cycle) with AA in the COX site equals approximately zero in contrast to the corresponding constant k_5 in reaction 9 and 50 of Tyr385*

reduction in states E_5 (COX_1 cycle) and E_{15} (COX_2 cycle) with the empty COX site (Table 2). It seems that AA in the COX site does not permit RC to react with Tyr385*. For similar reaction

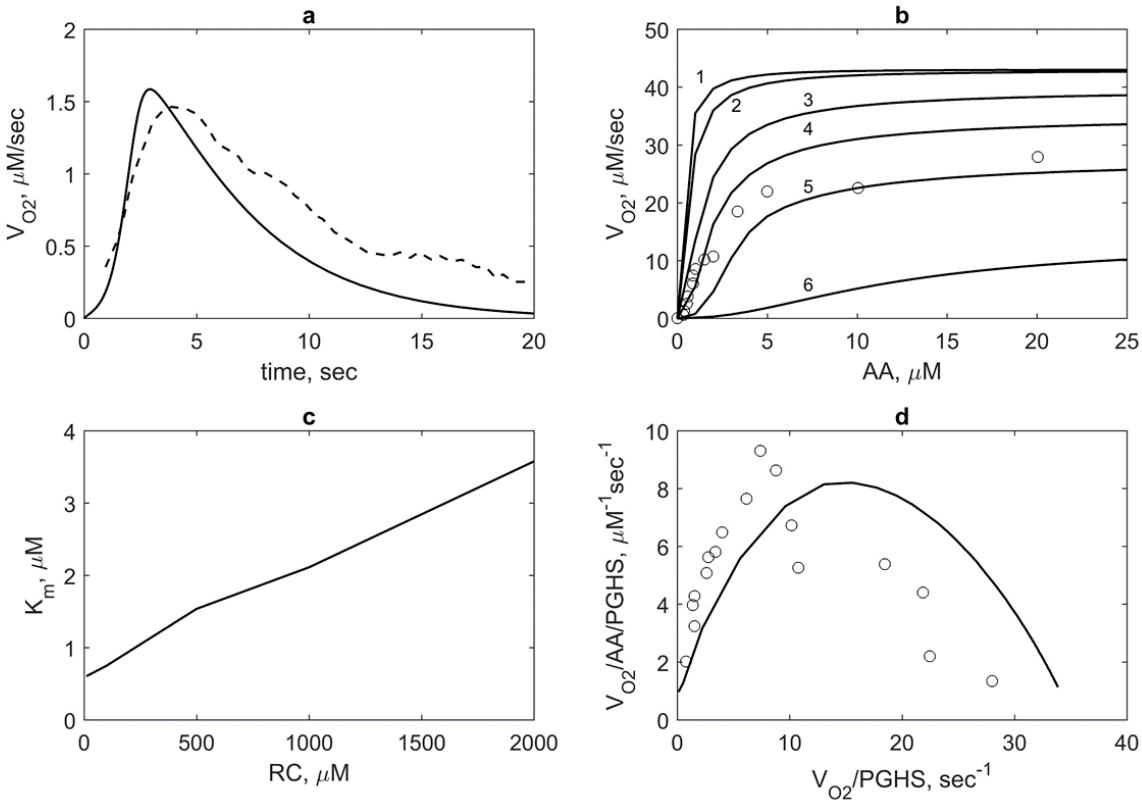

Fig. 6. Model validation based on experimental data on oxygen consumption by PGHS-1. (a) Theoretical (solid line) and experimental (dash line) dependence of oxygen consumption rate $V_{O2}(t)$: theoretical results obtained at 0.035 μM PGHS-1, 80 μM AA, and 300 μM RC; experimental data obtained at 0.035 μM PGHS-1, 80 μM AA and 100 μM ferulic acid [24]. *(b) Dependence of oxygen consumption V_{O2} on AA concentration calculated at 10 μM (line 1), 100 μM (line 2), 500 μM (line 3), 1000 μM (line 4), 2000 μM (line 5), and 5000 μM (line 6); 1000 μM phenol; points – experimental data obtained at 1000 μM phenol and 0.005 μM PGHS-1* [4]. *(c) Dependence of apparent Michaelis constant K_m of AA substrate on RC concentration calculated based on the data depicted in Fig. 6b. (d) the Eadie-Scatchard plot of value V_{O2}/AA/PGHS on value V_{O2}/PGHS. Lines and points – theoretical and experimental results obtained at the conditions provided in Fig. 6b.*

49 of Tyr385* reduction in states E_4 (POX_2-cycle) with PGG2* in the COX site, the constant equals k_5, that may mean that RC can reduce two radicals state in the COX site.

An increase of K_m with increasing RC concentration is accompanied by a change in a curve shape of $V_{O2}(AA)$ from hyperbolic to the sigmoidal one at high RC concentrations (Fig. 6b). To investigate this positive cooperativity in PGHS-1 function, we plotted the Eadie-Scatchard dependence of ratio $V_{O2}/AA/PGHS$ on $V_{O2}/PGHS$ (Fig. 6d) and provided the corresponding experimental data [4]. As seen, the theoretical downward-concave curve $V_{O2}/AA/PGHS$ vs. $V_{O2}/PGHS$ significantly differs from the linear Eadie-Scatchard plot

corresponding to Michaelis kinetics ($V_{O2}/AA = -V_{O2}/K_m + V_{max}/K_m$) that confirmed positive cooperativity in COX activity of PGHS-1 [21].

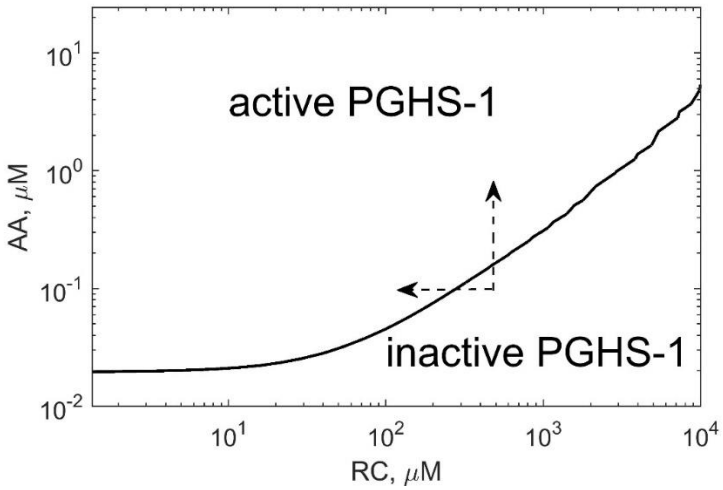

Fig. 7. The activation threshold of PGHS-1 depending on AA and RC concentrations. The curve corresponds to PGH_2 concentration level of 0.02 μM.

Positive cooperativity in the COX reactions defines the activation threshold of the PGHS-1 catalysis which depends on both AA and RC concentrations [4], [9]. Fig. 7 shows the activation threshold curve on a plan of AA and RC concentrations which divides the range of AA and RC concentrations on two regions, i.e. PGHS-1 is inactive at values of AA and RC concentrations lying below the curve and the enzyme is active in the range upper the curve. Increasing activation threshold at increasing RC concentration is determined by inhibition of the autocatalytic COX reaction by RC. The PGHS-1 kinetics at AA and RC concentrations far from the activation boundary is close to classical Michaelis-Menten kinetics that is typical for *in vitro* experiments on PGHS-1 kinetics and its inhibition by NSAIDs. Nonlinear effect in PGHS-1 kinetics becomes more pronounced near the activation threshold, in the range of low AA concentrations (50 nM – 1 μM) which are likely to relate to cellular conditions [19]. Below this boundary the PGHS-1 is in latent state and can be activated either increasing AA or decreasing RC concentrations as shown by arrows in Fig. 7.

2.6. RC effect on COX activity

We also applied our model to describe experimental data on the effect of RC on the oxygen consumption by PGHS-1 [2]. The results of calculation along with experimental data on the oxygen consumption rate, V_{O2}, depending on phenol concentration are shown in Fig. 8a. The

experimental and theoretical data were normalized to the control values obtained in the absence of RC. As seen, RC practically does not affect the oxygen consumption rate at RC concentration less than 1 mM and considerably inhibits COX activity at RC concentration higher than 1 mM.

For the comparison of these theoretical results with experimental data we used experimental data corrected for oxygen electrode signal [2]. Note that these data shows a slight increase of V_{O2}, approximately at 20 % above the control values in the comparison with uncorrected data [2] and data obtained by another group [10] which have the pick of V_{O2} about 2-3 times the control value. Our result showing no stimulation effect of RC on the COX reaction are closer to the corrected experimental and theoretical data [2].

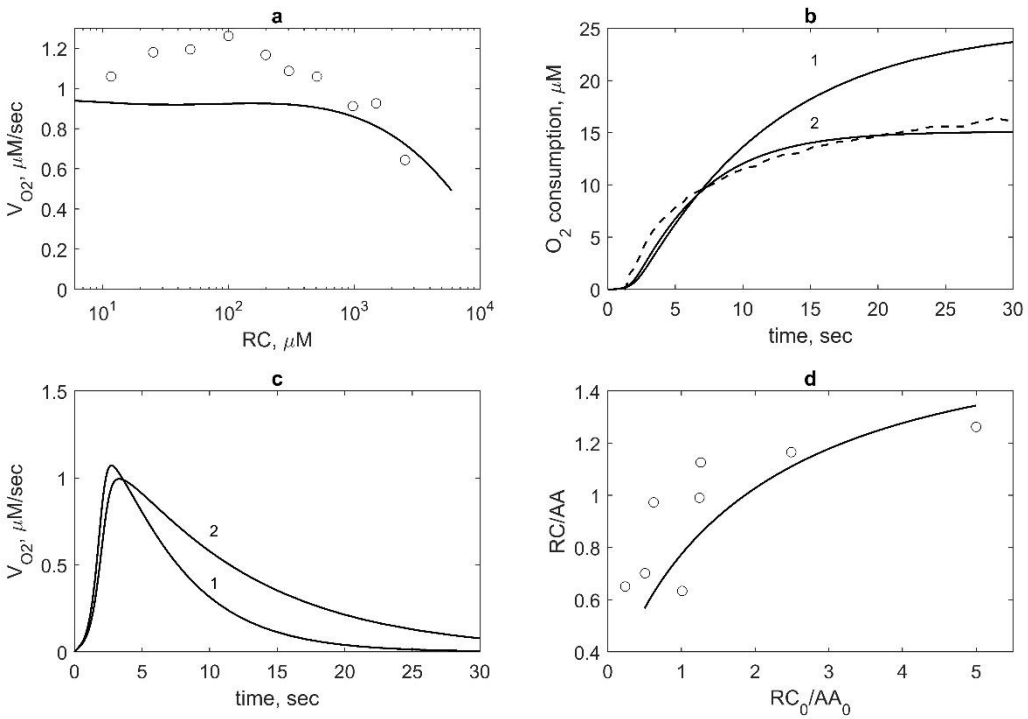

Fig. 8. Model validation based on the experimental data on the RC (phenol) effect on PGHS-1 kinetics. (a) Theoretical (line) and experimental (points) [2] *dependence of oxygen consumption rate V_{O2} on RC concentration. V_{O2} is normalised by its value obtained in the absence of RC. Calculation and experiment were carried out at 47 nM PGHS-1 and 100 μM AA. (b) Theoretical (solid lines) and experimental (dash line) kinetics of oxygen consumption. Calculation was carried out at 47 nM PGHS-1, 100 μM AA, 1000 μM RC (line 1) and 200 μM RC (line 2). Experimental data were obtained at 47 nM PGHS-1, 100 μM AA, and 1 mM phenol* [2]. *(c) Dependence of oxygen consumption rate V_{O2} calculated at 47 nM PGHS-1, 100 μM AA, 1 mM RC (line 1) and 200 μM RC (line 2). (d) Dependence of the ratio of RC and AA consumption, RC/AA, on the ratio of initial concentrations, RC_0/AA_0. Line – calculation at 35 nM PGHS-1 and points – experimental data obtained 35 nM PGHS-1, 20, 40, or 80 μM AA and 20, 50, or 100 μM ferulate* [24]. *The ratio RC/AA was given at 30 s after reaction initiation.*

According to our model, RC has an indirect stimulation effect on oxygen consumption. Calculation of O_2 consumption kinetics showed its increase at growing RC concentration (Fig. 8b). In the model the enhancement of O_2 consumption at RC concentration up to 1000 μM results from the extension of the functioning time of the enzyme due to its protecting from SI by RC. Increasing of the functioning time of PGHS-1 is seen well in Fig. 8c where time dependence of V_{O2} at different RC concentrations is shown.

2.7. Analysis of the connection between COX and POX activities

To analyse how our model describe stoichiometry between cosubstrate oxidation and arachidonic acid oxygenation during PGHS-1 functioning, we calculated dependence of the ratio between the rate of cosubstrate (phenol) and arachidonate consumption, RC/AA, on the ratio between their initial concentrations, RC_0/AA_0. Comparison of the theoretical results with experimental data [24] are shown in Fig. 8d.

The dependence of RC/AA shows the extent of the interconnection between the POX and COX cycles in the course of PGHS-1 function. The obtained ratio RC/AA is ranged from 0.5 to 1.3 that is consistent with the experimental range (0.6-1.3) [24]99], when RC/AA is in the region of 0.5 - 5. The theoretical data agree with prediction of the BC mechanism of PGHS-1 catalysis (0-2) [24], [26]. In our calculation, the dependence of RC/AA on RC_0/AA_0 is the dependence with saturation rather than linear dependence [24].

As AA consumption defines PGG_2 production, and RC consumption relates to PGH_2 synthesis, the ratio RC/AA determines the extent of the PGG_2 conversion to PGH_2. Because complete conversion of PGG_2 to PGH_2 requires 2 molecules of RC (RC/AA=2), the obtained value of the ratio RC/AA= 0.5-1.3 shows that POX cycles are slower than the COX ones and complete conversion of PGG_2 is not reached. Thus, according to the model some fraction of the intermediate product, PGG_2, remains in solution at the end of the catalytic cycle and is accumulated there. Note, the accumulation of PGG_2 in solution is proposed to be important for activation of PGHS-1 at cell stimulation.

3. Discussion

The microscopic network model of PGHS-1 developed on the base of a large amount of experimental data showed its capability to quantitatively describe the main kinetic properties of PGHS-1 under wide experimental conditions. The model also reproduced satisfactorily key

features of the complex PGHS-1 dynamics, i.e. interaction of COX and POX activities, processes of enzyme self-inactivation, its autocatalytic mechanism, and activation threshold of the enzyme. Correct description of these characteristics of PGHS-1 in the framework of self-consistent kinetic model with the unified set of kinetic parameters is critical for *in silico* screening and prediction of the NSAID inhibition effects in different experimental assays and targeted cells.

To validate and test predictive power of the model we applied it to the description of regulatory properties of the PGHS-1 and compared the results with additional experimental data not used in the calibration procedure. A study of the enzyme activity showed that AA and RC play various regulatory roles. We elucidated different mechanisms of inhibition and activation effects of RC on the enzyme. AA along with RC was shown to play activation role, switching the enzyme from an inactive state to the functioning one. In this case, RC was found to influence the activation threshold of the enzyme. Note that detailed understanding and description of these regulatory properties are important for the correct analysis of platelets activation as well as NSAID effects on this process.

The developed model was applied to study intermediate enzyme states and reactions which contribute significantly to the synthesis of PGG_2 and PGH_2. Taking into account two basic mechanisms of PGHS-1 function in the model, i.e. the Branched Chain [5], [24] and Tightly Coupled [1] mechanisms allowed us to estimate the contribution of each mechanism to the prostaglandin H2 biosynthesis.

The model supported the BC mechanism of PGHS-1 function, which assumes that Tyr385* radical in the COX site is a key component in interconnection between the COX and POX activities [24]. We also concluded that Tyr385* radical formation is required for effective binding of AA to the COX site. For AA to bind effectively, PGHS-1 first should be activated by a formation of Tyr385* radical due to POX activity of the enzyme. This effect is likely to result from a possible conformation change in the COX site by Tyr385* radical formation that can lead to an increase of the COX site affinity to AA. And vice versa, AA in the COX site can suppress Tyr385* radical formation. Note that experimental data indicates the possible mutual interaction between molecular compound in the COX site and Tyr385* radical formation. For example, experimental studies strongly indicate that the tyrosyl radical in inhibitor-treated PGHS-1 is probably not located at Tyr385 [28], and the alternative tyrosyl radical is not competent for COX catalysis. This data can serve an example of the effect of inhibitor molecules on the enzyme internal structure and dynamics particularly on the suppression of Tyr385* radical formation in the COX site [13].

As the result of the model fitting against of the experimental data, dissociation constants, $K_{d,1}$ of AA binding to the COX-site with Tyr385* radical states (E_5 and E_{15} in COX_1 and COX_2 cycles, respectively) was obtained to be lower than the corresponding constants, $K_{d,12}$ of AA binding to the states without Tyr385* radical state (E_1, E_2 and E_3 states in the POX_1 cycle, see Table 2). A negligible contribution of reactions 30-32 to the catalysis did not permit studying carefully the difference in dissociation constants of AA binding to various enzyme states. The additional experimental and theoretical investigations are needed for elucidation of the Tyr385* radical influence on enzyme affinity to AA.

The flux analysis of the network model showed the basic role of the COX_2 cycle, which includes the ferric state of the enzyme E_{15}, [Fe(III), PP]. This conclusion contradicts the inference on a main contribution of the ferril state, E_5, [Fe(IV), PP] in the COX_1 cycle which was made based on EPR experimental data [5]. This contradiction can be explained by the lower temperature in the EPR experiment (-12°C) [5] than temperature (25 ^{o}C) in the acquisition of kinetic experimental data [14] used in the model calibration. The connectivity between the COX_1 and COX_2 cycles via reducing reactions 28 and 29 is assumed to decline due to lowering the rate constant of reducing reactions with decreasing temperature. It can lead to weakening of the COX_2 cycle contribution accompanied by increasing of the role of the COX_1 cycle.

As it has been noticed in section 2.1, we considered in the model an alternative mechanism of the COX reaction initiation which was proposed in the framework of the TC mechanism [1]. According to this mechanism, a direct hydrogen atom abstraction from AA by ferryl group of heme (reaction 56 from the E_{14} state in POX_4 cycle) occurs, when AA is in the COX site, and heme group is in ferril radical state (Compound I). The flux analysis allowed us to compare this mechanism of AA* radical formation with the alternative mechanism through Tyr385* radical, proposed in framework of the BC mechanism [5]. The obtained values of maximum reaction rates V_2 in the COX_1 cycle, V_6 in the COX_1 cycle, V_{64} from the E_{19} state, and V_{56} showed that the main mechanism of AA* radical formation is BC mechanism in comparison with TC mechanism. Thereby, the first stage of AA oxygenation including AA* radical formation occurs mainly due to Tyr385* reduction in accordance with the BC mechanism; the contribution of a direct hydrogen atom abstraction from AA by ferryl group of heme proposed in the TC mechanism is negligible in the model. On the other hand, the TC mechanism explains a significant contribution to PGG_2 production by the reaction of PGG_2* output from the E_4 state in the POX_4 cycle and its following reduction to PGG_2 in solution (reaction 57) proposed in the framework of the TC mechanism.

To investigate the inhibition role of RC we calculated the dependence of the apparent Michaelis constant K_m(RC) for AA on RC concentration and showed an increase K_m with increasing RC concentration. We also showed that the K_m(RC) dependence can be used in estimation of dissociation constant $K_{d,1}$ for AA binding to the enzyme. Dissociation constant $K_{d,1}$ ≈0.2 μM defined from the K_m(RC) dependence is close to that obtained in the fitting procedure (Table 2). The dissociation constant $K_{d,1}$ is important for its comparison with dissociation constants of different NSAIDs to estimate their competition for the COX site and correct analysis of IC_{50} of the different drugs in various experimental conditions [6]. It is to be noted that there are not any reliable data on RC nature and its concentration in different cells and *in vitro* measurements of the dose dependence for NSAIDs are usually carried out at high RC concentration (e.g. 1 mM of phenol). A change in the apparent Michaelis constant K_m for AA under RC concentration variation obtained in this calculation affects the values of IC_{50} for drugs measured at different RC and peroxide concentrations [7].

The inhibition effect of RC on PGHS-1 catalysis observed in the model at high concentration of RC (>1 mM, Fig. 8a) and can be explained by RC competition for Tyr385* radical in the COX site. RC molecular (e.g. phenol) is likely to be able to penetrate the COX-site and reduce Tyr385* radical that abrogates oxygenation reaction. Note that the same mechanism was proposed for interaction of nitric oxide with PGHS-1, i.e. •NO can terminate the COX activity by its reaction with Tyr385* radical forming 3-nitrotyrosine [18]. The same mechanism is suggested to explain an inhibition effect of phenolic antioxidant, acetaminophen (paracetamol) which can be realized concomitantly with its direct inhibition of the POX activity acting as reducing cosubstrate for the peroxidase protoporphyrin and preventing tyrosine radical formation in the COX site [17].

According to experimental data, RC also causes a stimulation effect on PGHS-1 catalysis at low RC concentration [10], [17]. Our model partly explained the stimulation mechanism of RC (phenol, acetaminophen and others) by the following processes. First, RC was showed to prevent the enzyme from suicide inactivation resulting from its damage by radicals and extend the catalytic time of PGHS-1 (Figs. 3a, 3b and 8b). Second, in the model, RC reduces PGG2* inside of the COX site that can occurs according to the TC mechanism (reactions 4 and 57 in the COX_1 and POX_2 cycles, respectively). The further extension of the current model is required to study the stimulation role of RC in PGHS-1 catalysis.

Analysis of the oxygen consumption dependence on substrate and co-substrate concentrations showed its sigmoidal shape in the range of low AA and high RC concentrations (Fig. 6b) that points at positive cooperativity and nonlinear mechanism in the enzyme

functioning. Positive cooperativity in the enzyme kinetics is also confirmed by the calculation of the Eadie-Scatchard plot that significantly differs from linear dependence and has downward-concave shape (Fig. 6d). The molecular mechanic of positive cooperativity of PGHS-1 function is not entirely understood. In the case of dimer structure of PGHS-1, a possible mechanism of cooperativity can be determined by either allosteric interaction between two subunits of the holoenzyme or cooperativity within each monomer [10], [21]. In our model, we proposed independent function of the PGHS-1 monomers, thus manifestation of cooperativity in the model does not connected with its dimer structure. An increase in the cooperativity extent with increasing RC and decreasing AA concentrations suggested that the POX activity and the reducing co-substrate concentration are determinant factors in positive cooperativity in the COX reactions. As cooperativity in the COX activity is observed profoundly close to the activation threshold of PGHS-1, the cooperativity is linked to the autocatalytic effect of AA on the COX reactions through a positive feedback via the POX cycle which is activated at high RC concentrations. Note that the positive cooperativity and noticeable activation threshold are absent in the inducible PGHS-2 isoform whose kinetics is closer to the classical Michaelis-Menten one [9], [21]. This difference in initiation kinetics of two isoforms of PGHSs in the range of cellular submiromolar concentration of AA suggests a different control mechanism in prostaglandin biosynthesis by constitutive PGHS-1 and inducible PGHS-2 which both consume the same substrate and cosubstrate. In case of constitutive PGHS-1, the activation threshold adjustable to cellular conditions ensures a fast activation of latent enzymes and their inactivation by triggering of AA concentration to cellular demands nearby the activation threshold. The lower activation threshold and the absence of positive cooperativity in initiation kinetic of PGHS-2 guarantees a fast and strong response of the enzyme to the cellular stimulus [9]. It is proposed that distinctive regulatory properties of two isoforms of PGHSs reflect their different physiological roles in the same cells expressing both PGHS-1 and PGHS-2.

4. Methods

4.1. Parametrisation of the PGHS-1 model

In accordance with the developed scheme for the PGHS-1 catalytic cycle (Fig. 2) we developed a kinetic model for PGHS-1 catalysis. The model includes 28 ordinary differential equations (ODEs) formulated for 24 enzyme catalytic states (E_i) and six metabolite

concentrations (AA, O_2, RC, OC, PGG_2, and PGH_2). The whole system of ODEs and conservation laws are presented in Supplementary Materials. To run numerical simulation and calibration of the model we used the software package for kinetic modelling DBsolve 6.1 [8] and the Systems Biology Toolbox for MATLAB (Mathworks).

The reaction rate expressions for all the reactions were formulated according to the mass action law with the rate constants being the parameters of the model (see Supplementary Materials). To identify the model parameters, we fitted the solutions of the ODEs against the experimental data on enzyme kinetics of PGHS-1 available from the literature.

The model includes 66 reactions and 68 corresponding reaction rate constants. The experimental data published in literature are not sufficient for reliable identification of all the model parameters. The lack of the data is mainly due to some peculiarities of the experimental design generally used for kinetic studies of PGHS-1 catalysis. The majority of such experimental studies included the time course for metabolite concentrations or reaction rates of their consumption or production such as AA or O_2 consumption, RC oxidation, and PGH_2 production. Whereas these characteristics are relatively easy to study experimentally, the measurement of kinetic dependencies for individual enzyme intermediates (catalytic states E_i in our model) requires development of sophisticated experimental techniques and often can be practically impossible. For example, experimental distinguishing of different radical states represents a special difficult task [29]. To reliably identify 68 reaction rate constants, we would ideally need time series data for the majority of enzyme catalytic states considered in the model. Taking into account lack of such the data we propose the following way to reduce the number of parameters in the model.

In general, all the reactions in the developed catalytic cycle can be classified into several groups, as some of them are of similar types. For example, we grouped together the reactions of AA binding to the COX site (reactions 1, 30, 31, and others), or reduction of PGG_2 to PGH_2 (reactions 11, 16, 20, and others). The reactions within the groups differ from each other by the enzyme catalytic state participating in corresponding reactions. For example, AA can bind to the enzyme being in resting state [Fe(III), PP, Tyr] (E_1, reaction 31) and ferryl states [Fe(IV), PP, Tyr] and [Fe(IV), PP*+, Tyr] (E_3 and E_2 states in reactions 30 and 32, respectively). Alternatively, AA can bind to the enzyme state containing Tyr385 radical (E_5, E_{15} and E_{11} states; reactions 1, 5 and 47, respectively). Therefore, it was assumed that the reactions of similar type would have similar rate constants.

However, in general case kinetic constants of the elementary reactions taking place in one of the catalytic sites can depend on the state of all other catalytic components, located in the

nearest proximity and involved in the further catalytic steps. For example, there are experimental evidences that AA binding to the COX site may depend on the presence/absence of the radical on Tyr385 [11]. PGHS-1 is a bifunctional enzyme and though the reactions traditionally referred to as COX activity and POX activity are catalysed in different sites, there are indications that the processes in one site can influence the rate of the processes in the other one. This phenomenon is traditionally discussed in the context of cooperativity of PGHS-1 [2].

We tried different approaches in grouping the model parameters and analysed the results of fitting of the corresponding models to the same set of experimental data. Analysis of the fitting results allowed us to hypothesise which reaction rates do not depend much on the processes taking place in the neighbour site, and therefore to conclude, which kinetic constants can be assumed to be equal to each other. This analysis also allowed us to make conclusions on the cooperativity between COX and POX activities. The approach we used finally allowed significantly reducing the number of parameters subject to fitting. The best fitting of the model to experimental data was achieved with the set of 18 parameters, given in Table 2 and further discussed in the text.

When identifying the model parameters, we were pursuing the goal to find a unified set of parameters, which would allow consistently describing a majority of *in vitro* kinetic data known for PGHS-1 catalysis. Identification of the model parameters and their further validation was performed as follows. We have chosen several experimental data sets obtained in different research laboratories to fit the model parameters against the data, and then validated the calibrated model by checking its applicability to the description of experimental data which were not taken in the fitting procedure.

To avoid ambiguity, for the initial stage of the fitting, among all kinetic information available for PGHS-1, we have chosen three datasets, which were obtained for the same object, purified PGHS-1 from sheep seminal vesicles, under approximately the same experimental conditions (temperature and pH). The first set included kinetic data on PGG_2 and PGH_2 production (points in Figs. 3a and 3b) measured at the different concentration of RC, phenol [24]. As the second dataset, we used the kinetic data on AA consumption (points in Fig. 3c), obtained for the different AA concentrations at the fixed concentration of RC, phenol [4]. The third dataset included kinetics of RC oxidation (adrenaline) at various concentrations of the enzyme [23].

4.2. Global sensitivity analysis of the model

Global sensitivity analysis (GSA) of the model to the kinetic parameters obtained in the fitting procedure was based on Morris GSA method of the calculation of the elementary effects [3, 16]. The resulting Morris ranking is calculated as

$$Ranking = (\mu^2 + \sigma^2)^{1/2},$$

where μ and σ are two sensitivity measures in Morris GSA method, i.e. μ assesses the impact of a parameter on the model output and σ describes the non-linear effects and interactions of the parameters. As the model output in the calculation, we took an area under the curve (AUC) of PGH_2 time course.

5. Conclusion

The key aim of this work was the development of reliable and validated kinetic model of PGHS-1 which reproduces main features of its complex kinetics and can be used as a computational tool for accurate prediction of inhibition effect of NSAIDs and their combinations in a range of cellular conditions. The developed network model integrates both the current models of molecular mechanism of PGHS-1 catalysis and a large dataset of experimental data on the kinetics and regulatory properties of PGHS-1. This integrative approach helped us to overcome the limitation of the previously developed PGHS-1 models mainly applicable to the description of specific *in vitro* data in a narrow range of substrate and cosubstarte concentrations.

The developed model of PGHS-1 is a platform for the further development of the kinetic model of inducible isoform PGHS-2 (COX-2) which is expressed together with PGHS-1 in vascular endothelia cells and other organs and is a target of COX-2 selective NSAIDs. Development of the kinetics models of two isoforms within the unified integrative approach would allow investigation of the different physiological roles of these isoforms in the same cells and analysis of NSAID inhibition effect on the balance of pro-thrombotic (thromboxane) and anti-thrombotic (prostacyclin) prostaglandins in platelets and endothelial cells.

Supplementary Materials:

Supplementary material contains the ODEs of the PGHS-1 model.

Acknowledgement

We acknowledge Dr Galina Lebedeva and Dr Oleg Demin for fruitful discussion and suggestions on the modelling strategy.

Author Contributions:

Conceptualization, AG and YK; Methodology, AG and YK; Software, AG and MS; Validation, AG; Formal Analysis, KP; Investigation, AG, YK, MS, and KP; Data Curation, KP; Writing – Original Draft Preparation, AG; Writing – Review & Editing, AG, YK, MS, and KP; Visualization, MS; Supervision, YK; Project Administration, KP.

Conflicts of Interest:

The authors report no conflict of interest.

References

1. Bakovic, M., Dunford, H.B.: Intimate relation between cyclooxygenase and peroxidase activities of prostaglandin H synthase. Peroxidase reaction of ferulic acid and its influence on the reaction of arachidonic acid. Biochemistry. 33, 21, 6475–82 (1994). https://doi.org/10.1021/bi00187a013.
2. Bambai, B.: Prostaglandin H synthase: effects of peroxidase cosubstrates on cyclooxygenase velocity. J. Biol. Chem. (2000). https://doi.org/10.1074/jbc.M003982200.
3. Campolongo, F. et al.: An effective screening design for sensitivity analysis of large models. Environ. Model. Softw. 22, 10, 1509–1518 (2007). https://doi.org/10.1016/j.envsoft.2006.10.004.
4. Chen, W. et al.: Hydroperoxide Dependence and Cooperative Cyclooxygenase Kinetics in Prostaglandin H Synthase-1 and -2. J. Biol. Chem. 274, 29, 20301–20306 (1999). https://doi.org/10.1074/JBC.274.29.20301.
5. Dietz, R. et al.: Higher oxidation states of prostaglandin H synthase: Rapid electronic spectroscopy detected two spectral intermediates during the peroxidase reaction with prostaglandin G2. Eur. J. Biochem. 171, 1–2, 321–328 (1988). https://doi.org/10.1111/j.1432-1033.1988.tb13793.x.
6. Goltsov, A. et al.: In Silico Screening of Nonsteroidal Anti-Inflammatory Drugs and Their Combined Action on Prostaglandin H Synthase-1. Pharmaceuticals. 3, 7, 2059–2081 (2010). https://doi.org/10.3390/ph3072059.
7. Goltsov, A. et al.: Kinetic modelling of NSAID action on COX-1: Focus on in vitro/in vivo aspects and drug combinations. Eur. J. Pharm. Sci. 36, 1, 122–136 (2009). https://doi.org/10.1016/j.ejps.2008.10.015.
8. Goryanin, I. et al.: Mathematical simulation and analysis of cellular metabolism and regulation. Bioinformatics. 15, 9, 749–758 (1999). https://doi.org/10.1093/bioinformatics/15.9.749.
9. Hazelton, W.D. et al.: Prostaglandin H synthases: members of a class of quasi-linear threshold switches. Biochem. Pharmacol. 68, 3, 423–432 (2004). https://doi.org/10.1016/J.BCP.2004.04.001.
10. Hsuanyu, Y., Dunford, H.B.: Prostaglandin H synthase kinetics. The effect of

substituted phenols on cyclooxygenase activity and the substituent effect on phenolic peroxidatic activity. J. Biol. Chem. 267, 25, 17649–57 (1992).

11. Kulmacz, R.J. et al.: Comparison of the properties of prostaglandin H synthase-1 and -2. Prog. Lipid Res. 42, 5, 377–404 (2003). https://doi.org/10.1016/S0163-7827(03)00023-7.
12. Kulmacz, R.J. et al.: Interaction between peroxidase and cyclooxygenase activities in prostaglandin-endoperoxide synthase. Interpretation of reaction kinetics. J. Biol. Chem. 269, 8, 5527–5536 (1994).
13. Kulmacz, R.J. et al.: Prostaglandin H Synthase: Perturbation of the Tyrosyl Radical as a Probe of Anti-Cyclooxygenase Agents. In: Prostaglandins, Leukotrienes, Lipoxins, and PAF. pp. 399–407 Springer US, Boston, MA (1991). https://doi.org/10.1007/978-1-4899-0727-1_38.
14. Lu, G. et al.: Comparison of the peroxidase reaction kinetics of prostaglandin H synthase-1 and -2. J. Biol. Chem. 274, 23, 16162–7 (1999). https://doi.org/10.1074/jbc.274.23.16162.
15. Mitchell, J.A. et al.: Cyclooxygenases and the cardiovascular system. Pharmacol. Ther. 107624 (2020). https://doi.org/10.1016/J.PHARMTHERA.2020.107624.
16. Morris, M.D.: Factorial sampling plans for preliminary computational experiments. Technometrics. 33, 2, 161–174 (1991). https://doi.org/10.1080/00401706.1991.10484804.
17. Nam, T.-G. et al.: Pyridine and pyrimidine analogs of acetaminophen as inhibitors of lipid peroxidation and cyclooxygenase and lipoxygenase catalysis. Org. Biomol. Chem. 7, 24, 5103–12 (2009). https://doi.org/10.1039/b912528k.
18. O'Donnell, V.B. et al.: Catalytic Consumption of Nitric Oxide by Prostaglandin H Synthase-1 Regulates Platelet Function. J. Biol. Chem. 275, 49, 38239–38244 (2000). https://doi.org/10.1074/JBC.M001802200.
19. Smith, W.L. et al.: Cyclooxygenases: Structural, Cellular, and Molecular Biology. Annu. Rev. Biochem. 69, 1, 145–182 (2000). https://doi.org/10.1146/annurev.biochem.69.1.145.
20. Song, I. et al.: Different suicide inactivation processes for the peroxidase and cyclooxygenase activities of prostaglandin endoperoxide H synthase-1. Biochem. Biophys. Res. Commun. 289, 4, 869–875 (2001). https://doi.org/10.1006/bbrc.2001.6071.
21. Swinney, D.C. et al.: Differential Allosteric Regulation of Prostaglandin H Synthase 1

and 2 by Arachidonic Acid. J. Biol. Chem. 272, 19, 12393–12398 (1997). https://doi.org/10.1074/jbc.272.19.12393.

22. Tsai, A.-L., Kulmacz, R.J.: Prostaglandin H synthase: Resolved and unresolved mechanistic issues. Arch. Biochem. Biophys. 493, 1, 103–124 (2010). https://doi.org/10.1016/j.abb.2009.08.019.
23. Vrzheshch, P. et al.: A Novel Approach to Distinguish Between Enzyme Mechanisms: Quasi-Steady-State Kinetic Analysis of the Prostaglandin H Synthase Peroxidase Reaction. Biochem. J. 372, Pt 3, (2003). https://doi.org/10.1042/BJ20030043.
24. Wei, C. et al.: Comparison of branched-chain and tightly coupled reaction mechanisms for prostaglandin H synthase. Biochemistry. 34, 26, 8499–8512 (1995). https://doi.org/10.1021/bi00026a034.
25. Wu, G. et al.: A mechanistic study of self-inactivation of the peroxidase activity in prostaglandin H synthase-1. J. Biol. Chem. 274, 14, 9231–9237 (1999). https://doi.org/10.1074/jbc.274.14.9231.
26. Wu, G. et al.: Cyclooxygenase Inactivation Kinetics during Reaction of Prostaglandin H Synthase-1 with Peroxide. Biochemistry. 42, 46, 13772–13777 (2003). https://doi.org/10.1021/bi035415m.
27. Wu, G. et al.: Oxyferryl heme and not tyrosyl radical is the likely culprit in prostaglandin H synthase-1 peroxidase inactivation. Biochemistry. 46, 2, 534–542 (2007). https://doi.org/10.1021/bi061859h.
28. Wu, G. et al.: Peroxidase self-inactivation in prostaglandin H synthase-1 pretreated with cyclooxygenase inhibitors or substituted with mangano protoporphyrin IX. J. Biol. Chem. 276, 23, 19879–88 (2001). https://doi.org/10.1074/jbc.M100628200.
29. Wu, G., Tsai, A.-L.: Dynamics of Radical Intermediates in Prostaglandin H Synthase-1 Cyclooxygenase Reactions is Modulated by Multiple Factors. Protein Pept. Lett. 23, 11, 1013–1023 (2016). https://doi.org/10.2174/0929866523666161007151812.